Evidence for Temperature-Dependent Electron Band Dispersion in Pentacene

N. Koch,[1,*] A. Vollmer,[2] I. Salzmann,[1] B. Nickel,[3,†] H. Weiss,[4] and J. P. Rabe[1]

[1]*Institut für Physik, Humboldt-Universität zu Berlin, Newtonstrasse 15, D-12489 Berlin, Germany*
[2]*Berliner Elektronenspeicherring-Gesellschaft für Synchrotronstrahlung m.b.H., D-12489 Berlin, Germany*
[3]*Department of Chemistry, Princeton University, Princeton, New Jersey 08544, USA*
[4]*Chemisches Institut, Otto-von-Guericke-Universität Magdeburg, D-39106 Magdeburg, Germany*

(Received 7 November 2005; published 19 April 2006)

Evidence for temperature-dependent electron band dispersion in a pentacene thin film polymorph on graphite is provided by angle- and energy-dependent ultraviolet photoelectron spectroscopy. The bands derived from the highest occupied molecular orbital exhibit dispersion of ~190 meV at room temperature, and ~240 meV at 120 K. Intermolecular electronic coupling in pentacene thin films is thus confirmed to be dependent on temperature and possibly crystal structure, as suggested by additional infrared absorption measurements.

DOI: 10.1103/PhysRevLett.96.156803 PACS numbers: 73.20.At, 68.55.−a, 71.20.−b

Introduction.—Huge fundamental and application-oriented research efforts are devoted to pentacene, one of the prototypical conjugated organic molecules forming van der Waals crystals. Thin films of pentacene can easily be obtained by vacuum sublimation, and depending on the deposition conditions the (co-) existence of several polymorphs has been reported [1–4]. Relatively high charge carrier mobilities have been reported for both single crystals (greater than 11 $cm^2/V\,s$) [5] and thin films (up to 5 $cm^2/V\,s$) [6,7]. The influence of intermolecular packing on electronic properties and charge transport has attracted strong interest, in particular, when considering the potential application in field-effect transistors [6,8]. While band-like transport has been reported for pentacene at low temperatures [5,9], the nature of charge transport at room temperature is still debated, since such measurements may be strongly influenced by a considerable density of defects [5,10,11]. Appreciable widths of the two valence electronic bands derived from the highest occupied molecular orbital (HOMO) (due to two pentacene molecules in the unit cell) have been predicted by several theoretical investigations [12–16], ranging from <0.2 eV [13,14] up to ~0.7 eV [12], depending on assumed crystal structure, crystal direction, and level of theory. Furthermore, a significant reduction of bandwidth induced by local and nonlocal electron-phonon coupling, accompanied by reduced intermolecular electron coupling matrix elements, at elevated temperatures have been predicted [17,18]. However, no experimental data on the predicted band dispersion in pentacene crystals or thin films are yet available.

We succeeded in growing a textured crystalline pentacene thin film of yet unsurpassed quality, where the long molecular axes are oriented parallel to the substrate surface. This enabled the use of angle-resolved and energy-dependent photoemission spectroscopy (PES) to study the dispersion of HOMO-derived bands. Here we provide evidence that these bands exhibit a width of ~190 meV at room temperature, and ~240 meV at 120 K in our pentacene polymorph.

Experimental.—PES experiments were performed at the end-station SurICat (beamline PM4) at the synchrotron light source BESSY GmbH (Berlin). The ultrahigh vacuum (UHV) system comprises interconnected sample preparation (base pressure: 1×10^{-8} mbar) and analysis (base pressure: 2×10^{-10} mbar) chambers. Photoemission spectra were collected with a hemispherical energy analyzer (Scienta SES 100) with an energy resolution of 140 meV and an angular resolution of ±2.5°. For better visibility, spectra are shown after 5-point averaging. The angle between incident ultraviolet light and the energy analyzer was constant at 60°. Excitation energy-dependent spectra were recorded at normal emission. The sample was rotated relative to the directions of excitation and detection for angle-dependent series. Pentacene (Aldrich) evaporation was realized in the preparation chamber from a resistively heated pinhole source. The films' mass thickness was 12 nm for all samples (monitored with a quartz microbalance), and the evaporation rate was 0.2 nm/min. As substrates we used native silicon oxide (Si wafer cleaned in H_2O_2(30%) + H_2SO_4(99.99%) (3:1), etched with HF, and reoxidized by exposure to oxygen at atmospheric pressure for 1 h), and *ex situ* cleaved highly oriented pyrolytic graphite (HOPG; GE Advanced Ceramics).

For infrared (IR) absorption measurements, pentacene films of 12 nm thickness were deposited onto the respective substrates in a separate preparation chamber (base pressure $<10^{-6}$ mbar) under conditions comparable to those above. The spectra were recorded with unpolarized light at a resolution of 1 cm^{-1} in reflection (HOPG) and transmittance (SiO_2) geometry, respectively, and ratioed against spectra of the bare substrates (evacuated FTIR spectrometer Bruker IFS66v, DTGS detector).

X-ray measurements were performed using a transportable UHV-growth chamber at beamline X10B, NSLS, Brookhaven [11]. Pentacene films have been deposited *in situ* (base pressure $< 10^{-7}$ mbar), and reflectivity scans have been recorded for various film thicknesses ranging from bare HOPG substrate to 9.5 nm pentacene.

Results and discussion.—The long axes of pentacene molecules in films grown on HOPG are oriented parallel to the substrate surface (lying-down phase), as inferred from x-ray diffraction measurements [Fig. 1(a)]. The bare substrate signal was subtracted from the reflectivity scans at various coverages, thus enhancing the visibility of the pentacene diffraction peak. The diffraction peak observed at $q = 1.70$ Å^{-1} corresponds to a lattice spacing of 3.70($\pm$0.02) Å. The same value was found for lying-down pentacene deposited on Ag(111) using the supersonic beam method [19], and for an in-plane spacing of pentacene deposited on amorphous carbon coated mica [20], in both cases assigned to the (200) diffraction peak. Note that this spacing is different from the respective values of a thin film phase commonly observed on SiO_2 (3.8 Å) [3,21], as well as the bulk value (3.95 Å) [3,21]. The present polymorph for pentacene/HOPG is therefore assigned to the crystal structure reported in Ref. [19], which is possibly orthorhombic [20]. The highly ordered growth proceeds for fairly large thicknesses, as can be seen from the thickness-dependence study. The HOPG substrate consists of small crystalline grains (several μm wide); the fiber axis is along the surface normal. Consequently, the pentacene film possesses a fiber texture with (100) as the fiber axis along the surface normal [19]; see inset of Fig. 1(a). The morphology of the film is characterized by large blocklike crystals with deep trenches [see atomic force microscopy (AFM) micrograph in Fig. 1(b)].

PES spectra of pentacene/HOPG recorded at a photon energy ($h\nu$) of 25 eV as a function of electron emission angle (θ_e) are shown in Fig. 2(a). The emission feature seen here is solely derived from the pentacene HOMO, the HOMO-1 being well separated at a binding energy (BE) of 2.6 eV. Dashed lines are intended for better visualization of the peak-maximum shift, which amounts to $\sim$50 $\pm$ 20 meV. Increasing θ_e from 0° leads to higher peak-maximum BE. However, for electron emission angles larger than 21°, the peak-maximum BE decreases again, reaching the value measured at $\theta_e = 0°$. In order to access higher electron wave number values perpendicular to the surface ($k_\perp$), i.e., along (100) of the pentacene crystal structure, $h\nu$ was incrementally increased, and PES spectra taken at $\theta_e = 0°$ [Fig. 2(b)]. The apparent peak center of gravity shifted towards lower BE for increasing $h\nu$, which can clearly be seen as the pronounced low BE peak shoulder, in particular, for $h\nu = 43$ eV. Larger photon energies led to a shift of the peak back towards higher BE. A peak fitting routine (program WINSPEC, developed at the University of Namur) yielded a total shift of 190 $\pm$ 50 meV. While peaks for the angle-dependent series [Fig. 2(a)] could be fitted with one symmetric Gaussian function, an increasingly asymmetric Gaussian function had to be used to yield satisfactory fits for photon energies larger than 33 eV in the energy-dependent series [Fig. 2(b)]. A summary of peak-maximum values obtained from this fitting routine is illustrated in Fig. 3(a). In addition to the results from measurements at room temperature, according values are shown for measurements performed with the sample at 120 $\pm$ 10 K (spectra not shown: the relatively small differences compared to room temperature measurements cannot be easily seen by eye). In order to plot angle- and energy-dependent results in one graph, the x axis was chosen as

$$E_{\mathrm{kin}}\cos^2\theta_e \tag{1}$$

where E_{kin} is the photoelectron kinetic energy. This value is proportional to $k_\perp^2$. We have chosen this representation, as $k_\perp$ can only be assessed by assuming a certain value of the pentacene inner potential V_0 (see below). In general, $k_\perp$ is given by [22]

$$k_\perp = (2m/\hbar^2)^{1/2}(E_{\mathrm{kin}}\cos^2\theta_e + V_0)^{1/2} \tag{2}$$

with m being the electron mass.

Notably, the observed HOMO bandwidth increased from $\sim$190 $\pm$ 50 meV at room temperature to $\sim$240 $\pm$ 50 meV

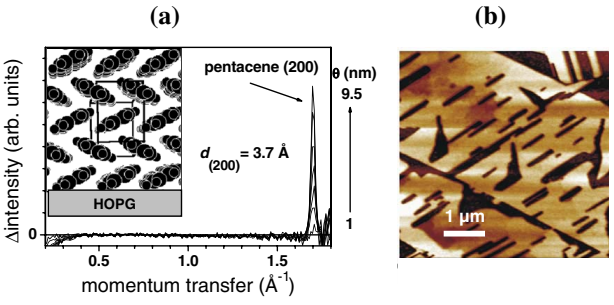

FIG. 1 (color online). (a) X-ray diffractogram of pentacene on HOPG for increasing thickness θ. The inset shows a schematic side view of pentacene molecule orientation on the substrate, and the crystallographic unit cell. (100) is oriented along the plot y axis. (b) Representative AFM image of a 12 nm thick pentacene film on HOPG (5×5 μm^2; z scale: 30 nm).

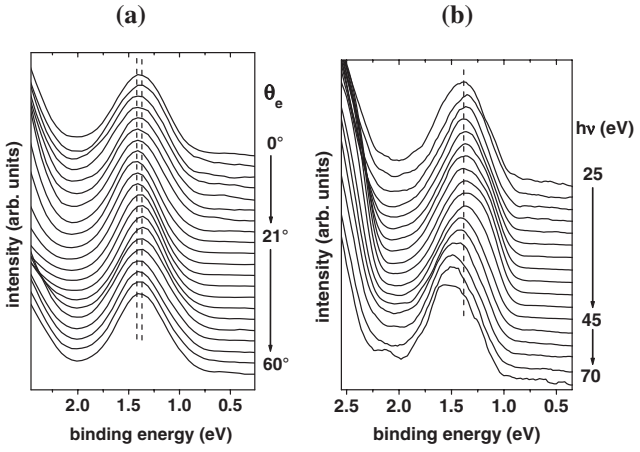

FIG. 2. Room temperature (a) angle-resolved and (b) energy-dependent photoemission spectra of the pentacene HOMO region (on HOPG). Binding energy is given relative to the Fermi level, set to zero.

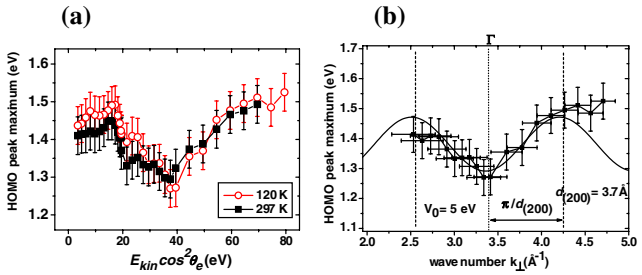

FIG. 3 (color online). (a) Summary of the HOMO-emission peak-maximum binding energies measured for pentacene/HOPG (spectra shown in Fig. 2) at room temperature and at 120 K. (b) Fit of Eq. (3) to the experimental data at 120 K. The error bars shown in (a) refer to the absolute error in BE, the symbol size indicates the error obtained for BE shifts of subsequent measurements.

at 120 K. This error refers to the absolute error in BE. The error for *BE shifts* observed for different sample temperatures was significantly smaller (± 20 meV). Note that this temperature-dependence of the bandwidth was observed for several samples, and was reversible for subsequent cooling-heating cycles. Our observations are in very good qualitative agreement with theoretical predictions [17], where the bandwidth was calculated as function of temperature. Increasing bandwidth is expected for decreasing temperature due to decreased population of intramolecular and intermolecular phonons disturbing the molecular crystal periodicity [17,18].

A detailed analysis of the dispersion measured at 120 K is shown in Fig. 3(b), using a simple tight-binding model that has already been successfully used to explain band dispersion in other organic materials [23–25], where the dispersion relation for the binding energy E_B is given by

$$E_B(k_\perp) = E_{B,0} - 2t\cos(a_\perp k_\perp) \qquad (3)$$

with $E_{B,0}$ the band center, t the transfer integral (containing local and nonlocal electron-phonon coupling effects), and $a_\perp$ the lattice spacing normal to the surface. For calculating $k_\perp$ [Eq. (2)] we used $V_0 = 5$ eV, which was found appropriate for a number of other organic materials [23,25]. $a_\perp$ is known as $d_{(200)}$ and was set to 3.7 Å. [Note that the present nonsymmorphic pentacene polymorph may have a glide plane. Consequently, final state selection rules lead to a doubling of the observed Brillouin zone, as was the case for graphite (0001) [26].] As can be seen from the figure, these parameters adequately describe the experimental data. Note that a clear-cut observation of the BE maxima at $k_\perp = 2.5$ Å^{-1} is hindered by the photon energy range available, which limits the minimal $k_\perp$ range. At $k_\perp > 4.25$ Å^{-1}, the deviation of the experimental data from the periodic band structure [solid curve in Fig. 3(b)] may be due to the fact that we evaluate the dispersion from the center of the photoemission peak. However, two bands might be contained within the rather broad emission peak observed. In addition, the limited angular resolution of the spectrometer may lead to an overestimation of BE values at large $k_\perp$ [25,27], as observed.

Frequently, silicon oxide is used as substrate for pentacene growth, mainly in the context of field-effect transistor fabrication. It is known that a fiber texture along the (001) direction prevails for pentacene/SiO_2 [8,28]; i.e., the pentacene long molecular axis is oriented almost vertically on the substrate. We performed angle- and energy-dependent PES studies on pentacene deposited on native silicon oxide, analogous to that reported for pentacene/HOPG above. Note that following our infrared spectroscopy investigations [Fig. 4(a)], pentacene/SiO_2 grows in a different polymorph than pentacene/HOPG. The peak positions of most vibrations differ in their energy by up to 9.5 cm^{-1}, thus indicating a different intermolecular interaction, and consequently different molecular packing and intermolecular electron coupling matrix elements. Similar shifts in intramolecular vibrational energies have been observed in Raman spectroscopy studies on two different pentacene polymorphs [29]. Furthermore, pentacene/SiO_2 almost exclusively grows in polymorphs characterized by c axes that are shorter than deduced here for pentacene/HOPG [21,28].

In PES, for pentacene/SiO_2 no angle- or energy-dependent BE shifts of the HOMO-derived emission—like the ones seen in Fig. 2—were observed, in agreement with theory [12,14,16]. Interestingly, in contrast to pentacene/HOPG, the HOMO-derived emission could only be fitted adequately with asymmetric Gaussian functions for virtually *all* angles and photon energies investigated [see line shape comparison Fig. 4(b)].

This behavior might be explained by assuming that the HOMO band dispersion is similar for both pentacene/SiO_2 (in plane) and pentacene/HOPG (perpendicular to the surface) [16]. In our experimental geometry, and with the present pentacene fiber texture, all electron wave vectors parallel to the substrate surface ($k_\parallel$) values are detected

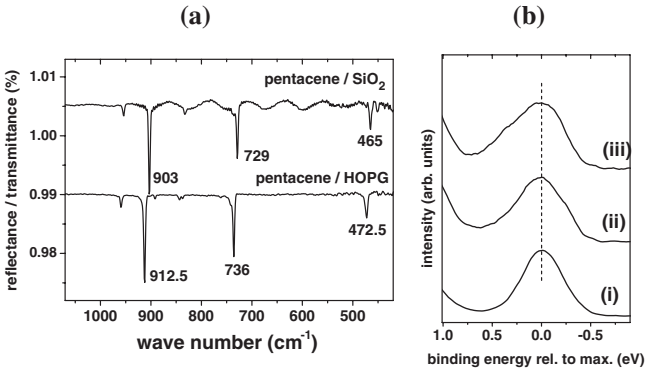

FIG. 4. (a) Infrared absorption spectra of 12 nm pentacene on HOPG and SiO_2. The three labeled peaks correspond to CH out-of-plane bending modes. (b) Comparison of the pentacene HOMO region PES line shape for (i) pentacene/HOPG $h\nu = 25$ eV, $\theta_e = 0°$, (ii) pentacene/HOPG $h\nu = 45$ eV, $\theta_e = 0°$, and (iii) pentacene/SiO_2 $h\nu = 25$ eV, $\theta_e = 0°$.

simultaneously, i.e., the resulting PES spectra recorded are consequently a superposition of all possible $k_{\|}$ values, yielding the observed highly asymmetric HOMO feature for pentacene/SiO_2.

However, the shift of IR bands toward higher energy for pentacene/HOPG suggests that intermolecular interactions are smaller for pentacene/SiO_2 compared to pentacene/HOPG [29]. This may lead to a significant decrease in bandwidth for the HOMO-derived emission. The asymmetric HOMO feature observed for pentacene/SiO_2 is then related to the strong intramolecular electron-phonon coupling in pentacene. Gas-phase and low temperature monolayer PES spectra of pentacene exhibit such an asymmetric line shape of the HOMO-derived emission due to electron-phonon coupling [30,31]. The reduction in intermolecular electronic coupling for the pentacene polymorph on SiO_2 then may lead to a Huang-Rhys parameter similar to pentacene in the gas phase [30].

Conclusion.—Angle- and energy-dependent PES spectra for pentacene grown on SiO_2 have shown the theoretically predicted absence of appreciable HOMO-derived band dispersion along the surface normal (i.e., almost along the long molecular axes). However, PES data for a pentacene polymorph grown on HOPG provided evidence for a HOMO-derived band dispersion of $\sim$190 meV at room temperature and $\sim$240 meV at 120 K (perpendicular to the long molecular axes). The mechanisms responsible for that observation may be attributed to reduced intermolecular coupling at elevated temperatures due to strong electron-phonon coupling [17]. The measured increase in bandwidth for reduced temperature confirms theoretical predictions, and supports the interpretation of transport measurements on a number of oligoacenes.

The authors thank F. M. Danisman and G. Scoles for support during XRD experiments (supported by DOE Contract No. DE-FG02-93ER45503), and T. Seyller (Universität Erlangen), O. Rader (BESSY), and R. Manzke (HU-Berlin) for helpful discussions. This work was supported by the Sonderforschungsbereich 448 (DFG).

*Corresponding author.
Email address: norbert.koch@physik.hu-berlin.de

†Present address: Ludwig-Maximilians-Universität München, Department für Physik & CeNS, D-80539 München, Germany.

[1] R. B. Campbell, J. M. Robertson, and J. Trotter, Acta Crystallogr. **15**, 289 (1962).
[2] C. D. Dimitrakopoulos, A. R. Brown, and A. Pomp, J. Appl. Phys. **80**, 2501 (1996).
[3] C. C. Mattheus *et al.*, Synth. Met. **138**, 475 (2003).
[4] C. C. Mattheus *et al.*, Acta Crystallogr. Sect. C **57**, 939 (2001).
[5] O. D. Jurchescu, J. Baas, and T. T. M. Palstra, Appl. Phys. Lett. **84**, 3061 (2004).
[6] T. W. Kelley *et al.*, Chem. Mater. **16**, 4413 (2004).
[7] N. Karl, Synth. Met. **133**, 649 (2003).
[8] C. D. Dimitrakopoulos and P. R. L. Malenfant, Adv. Mater. **14**, 99 (2002).
[9] O. Ostroverkhova *et al.*, Phys. Rev. B **71**, 035204 (2005).
[10] A. Di Carlo *et al.*, Appl. Phys. Lett. **86**, 263501 (2005).
[11] B. Nickel *et al.*, Phys. Rev. B **70**, 125401 (2004).
[12] Y. C. Cheng *et al.*, J. Chem. Phys. **118**, 3764 (2003).
[13] J. Cornil, J. P. Calbert, and J. L. Bredas, J. Am. Chem. Soc. **123**, 1250 (2001).
[14] R. G. Endres *et al.*, Comput. Mater. Sci. **29**, 362 (2004).
[15] M. L. Tiago, J. E. Northrup, and S. G. Louie, Phys. Rev. B **67**, 115212 (2003).
[16] A. Troisi and G. Orlandi, J. Phys. Chem. B **109**, 1849 (2005).
[17] K. Hannewald *et al.*, Phys. Rev. B **69**, 075211 (2004).
[18] W. Q. Deng and W. A. Goddard III, J. Phys. Chem. B **108**, 8614 (2004).
[19] L. Casalis *et al.*, Phys. Rev. Lett. **90**, 206101 (2003).
[20] L. F. Drummy and D. C. Martin, Adv. Mater. **17**, 903 (2005).
[21] R. Ruiz *et al.*, Appl. Phys. Lett. **85**, 4926 (2004).
[22] S. Hüfner, *Photoelectron Spectroscopy* (Springer-Verlag, Berlin, 1995).
[23] G. N. Gavrila *et al.*, Appl. Phys. Lett. **85**, 4657 (2004).
[24] S. Hasegawa *et al.*, J. Chem. Phys. **100**, 6969 (1994).
[25] H. Yamane *et al.*, Phys. Rev. B **68**, 033102 (2003).
[26] D. Pescia, A. R. Law, M. T. Johnson, and H. P. Hughes, Solid State Commun. **56**, 809 (1985).
[27] G. Gensterblum, J. Electron Spectrosc. Relat. Phenom. **81**, 89 (1996).
[28] R. Ruiz *et al.*, Chem. Mater. **16**, 4497 (2004).
[29] L. Farina *et al.*, Chem. Phys. Lett. **375**, 490 (2003).
[30] V. Coropceanu *et al.*, Phys. Rev. Lett. **89**, 275503 (2002).
[31] H. Yamane *et al.*, Phys. Rev. B **72**, 153412 (2005).